Non-contact Robust Respiration Detection By Using Radar-Depth Camera Sensor Fusion

Heng Zhao[1], Xiaomeng Gao[2], Xiaonan Jiang[1], Hong Hong[3] and Xiaoguang Liu[1]

***Abstract*— In this paper, a non-contact respiration detection scheme based on Doppler radar-depth camera sensor fusion has been proposed. A continuous-wave (CW) Doppler radar sensor and a depth camera are used to measure the respiratory motion separately. Then the Bayesian sensor fusion algorithm is used to estimate the cycle-to-cycle breathing rate. The experiments prove that the proposed fusion scheme can provide an accurate breathing rate estimation than using a single sensor. In particular, the proposed scheme can give a reasonable estimation even under the influence of body movement.**

***Clinical relevance*— This paper gives a new method for robust non-contact respiration detection.**

I. INTRODUCTION

Recently, the non-contact vital sign detection has become an emerging technology in our daily life. It frees the human body from the wires and electrodes used in conventional vital sign sensors. Among the various techniques, the Doppler radar-based and depth camera-based techniques are well investigated and proved to be effective for non-contact respiration detection [1], [2].

The radar sensor has been used for respiration detection since 1975 , and has become a hot research topic since 2000 [1]. Various radar systems, such as continuous wave (CW) Doppler radar, frequency modulated CW (FMCW) radar, stepped frequency CW (SFCW) radar and impulse radio (IR) ultra-wide-band (UWB) radar have been developed for respiration detection [3]. Considering the detection accuracy, design complexity and system cost, the CW Doppler radar is a good solution for sensing the respiratory signal. It can theoretically achieve the sub-millimeter accuracy for tiny displacement detection [4]. The research on Doppler radar-based respiration detection focuses not only on the breathing rate measurement but also some applications such as breathing disorder detection and gated lung cancer radiotherapy [5], [6]. However, the CW Doppler radar sensor is very sensitive to the body motion other than the motions caused by vital signs within its beam [7]. As a result, the breathing rate may be inaccurate when the random body movement exists.

*This work was supported by the Air Force STTR under Grant FA8650-19-P-6088.

[1]Heng Zhao, Xiaonan Jiang and Xiaoguang Liu are with Department of Electrical and Computer Engineering, University of California, Davis, CA, USA hezh@ucdavis.edu, xnjiang@ucdavis.edu, lxgliu@ucdavis.edu

[2]Xiaomeng Gao is with Cardiac Motion LLC, Sacramento, CA, USA xiaomeng.gao@cardiacmotion.com

[3]Hong Hong is with School of Electronic and Optical Engineering, Nanjing University of Science and Technology, Nanjing, China hongnju@njust.edu.cn

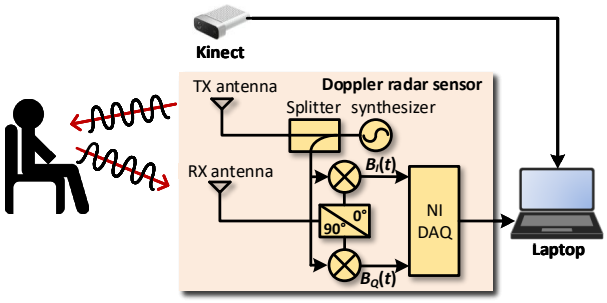

Fig. 1. Block diagram of the non-contact respiration detection scheme.

The video-based detection technique provides another effective method to remotely capture the respiratory motion. The depth camera can obtain the distance variation of each pixel within its field-of-view (FOV). Unlike the radar sensor, most of researchers focus on the optimizations of detection algorithm rather than the system [8], [9]. The detection of respiratory rate, respiratory waveform and volume change using depth camera have been reported in the literatures [8], [9].

In this paper, a novel non-contact detection scheme has been proposed for robust respiration detection. The Bayesian sensor fusion algorithm is utilized to combine the measurements from Doppler radar sensor and depth camera. The organization of this paper is shown below. The principles of Doppler radar sensor-based and depth camera-based respiration detection are introduced in Section II. Then the signal processing algorithm including signal preprocessing and Bayesian sensor fusion is discussed in Section III. Two experiments are presented in Section IV. Finally, a conclusion is given in Section V.

II. DESCRIPTION OF BASIC PRINCIPLES

Generally, the depth camera and CW Doppler radar both captures the torso displacement induced by respiration to measure the breathing activity. The Doppler radar sensor detects the Doppler frequency shift induced by the torso motion, while the depth camera records the depth value variation of the chest or abdomen regions. Their principles are described below.

A. Continuous Wave Doppler Radar

The block diagram of the CW Doppler radar is shown in Fig. 1. The radar sensor employs a homodyne architecture [10], which is widely used in non-contact vital sign detection due to its simplicity. For a typical homodyne architecture, the

radar transmits a single tone CW signal towards the human subject, the transmitted signal is reflected from his/her body and then received by the receiving antenna. The desired vital sign information is modulated in the phase of the received signal, which can be extracted through downconversion and spectral analysis.

In this custom-designed radar sensor, a pair of patch antennas are used as the transmitting and receiving antennas. The local oscillator (LO) signal is generated from a phase locked loop (PLL)-based synthesizer, whose frequency is 2.405 GHz. The transmitting power is 2 dBm. The LO signal is divided into two paths through the splitter. One is transmitted through the TX antenna, the other works as the LO signal for the mixer. The reflected signal is captured by the receiving antenna, and then fed to the mixer. A quadrature mixer is used here to downconvert the received signal to the baseband quadrature signals directly.

The in-phase and quadrature-phase signals can be written as

$$B_I(t) = DC_I + A\cos\left[\frac{4\pi x(t)}{\lambda} + \frac{4\pi D}{\lambda}\right] \tag{1}$$

$$B_Q(t) = DC_Q + A\sin\left[\frac{4\pi x(t)}{\lambda} + \frac{4\pi D}{\lambda}\right] \tag{2}$$

where DC_I and DC_Q are the dc offsets existed in the baseband signals, respectively. $x(t)$ denotes the measured chest wall motion. λ is the wavelength of the transmitted signal. D represents the nominal distance between radar and human subject. In practice, the dc offsets can be effectively eliminated by a circle fitting method, and the amplitude imbalance can be ignored. In order to extract the phase information, the arctangent demodulation is adopted, which is

$$\Phi(t) = \tan^{-1}\left[\frac{B_I(t)}{B_Q(t)}\right] = \frac{4\pi x(t)}{\lambda} + \frac{4\pi D}{\lambda} \tag{3}$$

The second term related to the nominal distance can be assumed as a constant value. As a result, the chest wall motion can be recovered from the phase information.

B. Depth Camera

We used an Azure Kinect development kit (DK) to obtain the depth information. The Azure Kinect DK includes a depth camera, an RGB camera, a spatial microphone array, and an orientation sensor.

The depth camera embedded in the Azure Kinect DK is based on the Amplitude Modulated Continuous Wave (AMCW) Time-of-Flight (ToF) principle. The depth camera emits the infrared radiation (IR) to the scene, and then records the time that travels from the camera to the scene and back. These measurements inside the field-of-view (FOV) are combined to generate a depth map, which is a set of Z-coordinate values from every pixel of the image.

Considering the operation principle of depth camera, the breathing activity can be obtained from the depth variation within the chest wall region during the breathing activity. In order to eliminate the outliers appeared in a single pixel, a proper region-of-interest (ROI) is necessary. Thus, the body tracking API is used to find the locations of the joints and determine the ROI adaptively. The locations of two joints, SPINE_NAVAL and SPINE_CHEST, are selected as the lower and upper borders, respectively. The width of ROI is determined as 0.8 time of height empirically. The time-domain respiratory signal is calculated by averaging the depth values of the pixels within ROI as

$$D(t) = \sum_{i=1}^{N_H}\sum_{j=1}^{N_W} P(i,j) \tag{4}$$

where N_W and N_H denotes the width and height of ROI, respectively. $P(i,j)$ represents the depth value of the pixel at the i-th row and j-th column in the depth map.

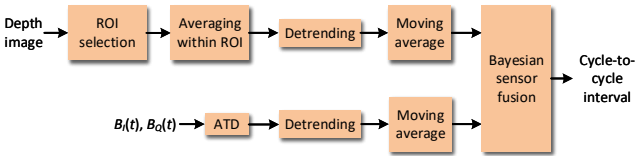

Fig. 2. Flow chart of the signal processing algorithm.

III. Signal Processing Algorithm

A. Signal Preprocessing

The simplified block diagram of the signal processing is shown in Fig. 2. The signal processing is realized in MATLAB. After arctangent demodulation, the outputs of the radar sensor contains the respiratory motion along with some motion artifacts and noise. First, a detrending process is used to eliminate the dc component and low-frequency drifting in the phase information. In order to remove the high-frequency noise and artifacts, a 100-point moving average filter is utilized. The peaks in the processed signal can be localized as $T_{radar} = [t_{radar}(1), t_{radar}(2), ..., t_{radar}(K)]$, the cycle-to-cycle intervals can be derived as

$$f_{radar}(i) = \frac{1}{t_{radar}(i+1) - t_{radar}(i)}, \tag{5}$$

where $i = 1, 2, ..., K-1$ are the index of sampling points.

Similar to the processing of radar signal, the output of depth camera firstly goes through a detrending process to remove the low-frequency components. Then a 100-point moving average filter is used to eliminate the high-frequency noise and artifacts. At last, the cycle-to-cycle intervals can be written as

$$f_{depth}(i) = \frac{1}{t_{depth}(i+1) - t_{depth}(i)}, \tag{6}$$

where $t_{depth}(i)$ is the peak location in each breathing cycle, and $i = 1, 2, ..., K-1$ are the index of sampling points.

B. Bayesian sensor fusion

Both radar sensor and depth camera can provide the cycle-to-cycle intervals of the respiratory signal. However, the respiratory signal can be smeared by artifacts such as random body movement. Therefore, a Bayesian sensor fusion is used

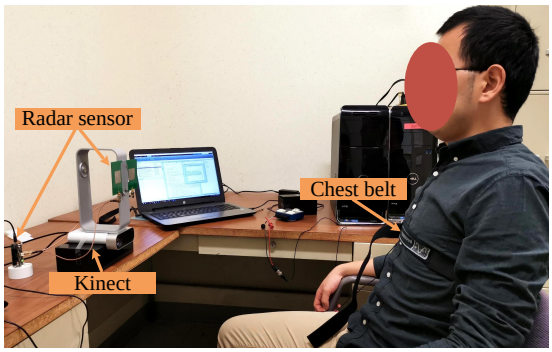

Fig. 3. The experimental setup.

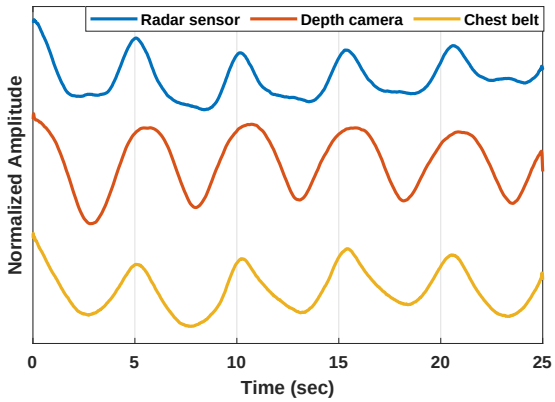

Fig. 4. The 25-s time-domain signals acquired from radar, depth camera and chest belt.

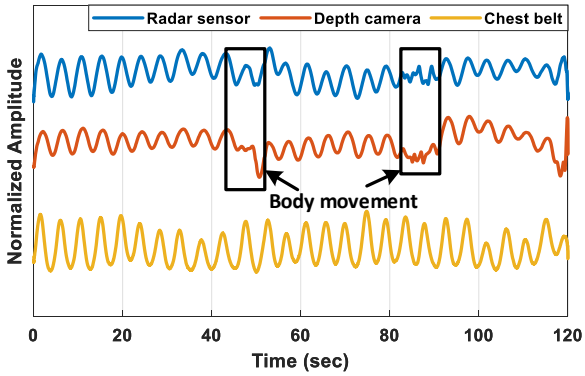

Fig. 5. The 120-s time-domain signal acquired from radar, depth camera and chest belt

to combine the results from the radar sensor and depth camera. The goal of the Bayesian fusion is to estimate the probability of the unknown state using the last measurements. That is to say, if the last measurements before artifacts from radar and depth camera are both determined, the current measurement which is contaminated by the artifacts can be estimated by the probability.

According to [11], assuming the k-th measurements from radar and depth camera are f_k^r and f_k^d, the probability density function (PDF) of the fusion output is [12]

$$p(f|f_k^r f_k^d) = \frac{p(f|f_k^r)p(f|f_k^d)p(f|f_{k-1}^r f_{k-1}^d)}{p(f|f_{k-1}^r)p(f|f_{k-1}^d)}, \quad (7)$$

where $p(f|f_k^r)$ and $p(f|f_k^d)$ denote the posterior PDF of radar sensor and depth camera, respectively. Since the only normal respiration is considered, the PDF derived from the cycle-to-cycle breathing rates in the last 25s is ideally regarded as a Gaussian distribution. As a result, the parameters σ and η can be estimated. The posterior PDF of a single sensor can be calculated as

$$p(f|f_k) = \frac{1}{\sqrt{2\pi}\sigma} e^{-\frac{1}{2}(\frac{f-f_k}{\sigma})^2}. \quad (8)$$

The fused cycle-to-cycle breathing rate after fusing the measurements from radar and depth camera can be determined by finding the peak value in the PDF.

IV. Experimental Validation

A. Experimental setup

Two sets of experiments were carried out to evaluate the proposed system. The experimental setup is shown in Fig. 3. The antennas and the camera were located at the same distance facing the chest wall of human subject. The human subject was asked to sit on a chair while leaning on the back during the experiments. A chest belt was used as the ground truth.

B. Comparison of Radar and Depth Camera

The first experiment was carried out to compare the performance of radar sensor and depth camera for respiration detection. The distance between the two sensors and the subject's chest wall is 80 cm. During the experiment, the human subject was asked to keep steady and breathed normally.

Fig. 4 illustrates the 25-s time-domain signals acquired from radar, depth camera and chest belt. In order to be consistent with the signals acquired from radar and depth camera, the same signal preprocessing procedure including detrending and moving average are used on the chest belt signal. It is obvious that the detected time-domain signals from radar and depth sensor both have good correlations in cycle-to-cycle intervals with the ground truth signal. It also should be mentioned that the signals acquired from the three sensors are noticeably different even though they all measure the motion on the chest wall. This is due to the different principles of the three sensors. The radar-detected signal can be regarded as the vector superposition of reflections from different scatters on the chest wall within the its beam. While the signal from depth camera is the direct summation of all pixels in the ROI. The chest belt senses the displacement under its sensor. Nevertheless, the activities of inhalation and exhalation can be identified clearly in each signal. Thus, both radar and depth camera can capture the respiratory signal accurately at the 80-cm range.

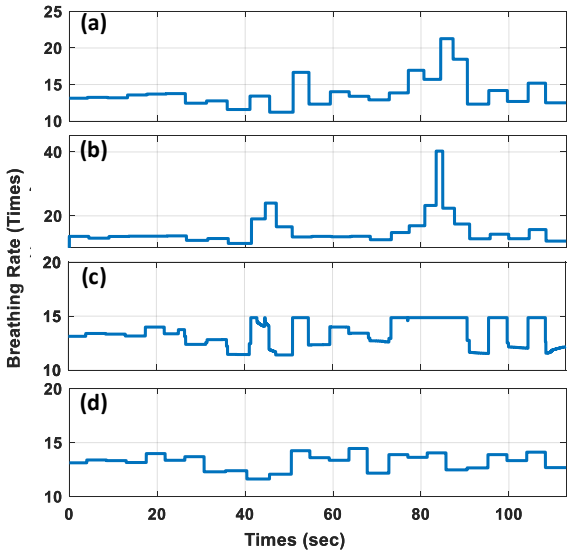

Fig. 6. Cycle-to-cycle breathing rate calculated from (a) radar, (b) depth camera, (c) Bayesian sensor fusion and (d) chest belt.

TABLE I
EFFECTIVE DETECTION RATIO FROM RADAR SENSOR, DEPTH CAMERA AND BAYESIAN SENSOR FUSION

Sensor type	Radar sensor	Depth camera	Sensor fusion
EDR	87.2 %	79.5 %	91.2 %

C. Fusion of Radar and Depth Camera

As proved in the last experiment, both radar sensor and depth camera can capture the respiratory motion. However, in practice, the signals from radar and depth camera may be smeared by the body movement. In the second experiment, the human subject was asked to breathing normally for 120 s while performing body movements twice. The experimental setup was same as the last experiment. The distance between the sensors and his chest wall is 80 cm.

Fig. 5 presents the time-domain signals acquired from radar sensor, depth camera and chest belt. It can be seen that the body movements occurred at 45th second and 85th second, which are highlighted by the black boxes. It can be seen that the radar-acquired and depth camera-acquired respiratory signals are smeared by the body movements severely. Their cycle-to-cycle breathing rates are shown in Fig. 6 (a) and Fig. 6 (b). We can see the outliers appear due to the unrecognizable peaks during the body movement. Fig. 6 (c) presents the cycle-to-cycle breathing rate after fusing the results acquired from radar and depth camera. Since the Bayesian fusion algorithm utilizes the probability of former data, the outliers can be eliminated by taking the probability of breathing rates calculated from measurements into consideration.

The effective detection rates (EDR) of two single sensors and fused result are shown in Table I. The EDR is defined as the ratio of measurements when the bias between measurement and ground truth is within 2 times per second. From this table, we know that the radar sensor has the higher EDR than the depth camera. The EDR improves after Bayesian sensor fusion, which demonstrates that the fusion algorithm is effective than using a single sensor. Furthermore, it is known from Fig. 6 that even though there is not much improvement of EDR, the Bayesian fusion can provide a more reasonable estimation when the body movement exists than single sensors.

V. CONCLUSIONS

A non-contact breathing detection scheme by fusing the radar sensor and depth camera has been proposed. The basic principles of radar-based and depth camera-based respiration detection have been introduced. Then the Bayesian sensor fusion algorithm has been used to combine the measurements from the two sensors. The experiments show that the proposed method can improve the effective detection rate and provide the reasonable cycle-to-cycle breathing rate estimation even under the influence of small scale body movement.

REFERENCES

[1] C. Li, Z. Peng, T. -Y. Huang, T. Fan, F. -K. Wang, T. -S. Horng, J. -M. Muñoz-Ferreras, R. Gomez-Garcia, and J. Lin, A Review on Recent Progress of Portable Short-Range Noncontact Microwave Radar Systems, IEEE Trans. Microw. Theory Techn., vol. 65, no. 5, pp. 1692-1706, Jan. 2017.

[2] A. Procházka, M. Schätz, O. Vyšata, and M. Vališ, Microsoft Kinect Visual and Depth Sensors for Breathing and Heart Rate Analysis, Sensors, vol. 16, no. 7, pp. 996, Jun. 2016.

[3] J. -M Muñoz-Ferreras, Z. Peng, R. Gomez-Garcia, and C. Li, Review on Advanced Short-Range Multimode Continuous-Wave Radar Architectures for Healthcare Applications, IEEE J. Electromagn., RF, Microw. Med. Biol., vol. 1, no. 1, pp. 14-25, Jun. 2017.

[4] J. Xu, X. Gao, B. E. Padasdao, and O. Boric-Lubecke, Estimation of Physiological Sub-millimeter Displacement with CW Doppler Radar, 2015 37th Annual International Conference of the IEEE Engineering in Medicine and Biology Society (EMBC), Italy, 2015.

[5] H. Zhao, H. Hong, D. Miao, Y. Li, H. Zhang, Y. Zhang, C. Li, and X. Zhu, A Noncontact Breathing Disorder Recognition System Using 2.4-GHz Digital-IF Doppler Radar, IEEE J. Biomed. Health Inform., vol. 21, no. 1, pp. 208-217, Jan. 2019.

[6] C. Gu, R. Li, H. Zhang, A. Y. C. Fung, C. Torres, S. B. Jiang, and C. Li, Accurate Respiration Measurement Using DC-Coupled Continuous-Wave Radar Sensor for Motion-Adaptive Cancer Radiotherapy, IEEE Trans. Biomed. Eng., vol. 59, no. 11, pp. 3117-3123, Nov. 2012.

[7] C. Li, and J. Lin, Random Body Movement Cancellation in Doppler Radar Vital Sign Detection, IEEE Trans. Microw. Theory Techn., vol. 56, no. 12, pp. 3143-4152, Dec. 2008,

[8] A. Procházka, H. Charvátová, O. Vyšata, J. Kopal, and J. Chambers, Breathing Analysis Using Thermal and Depth Imaging Camera Video Records, Sensors, vol. 17, no. 6, pp. 1408, Jun. 2017.

[9] V. Soleimani, M. Mirmehdi, D. Damen, J. Dodd, S. Hannuna, C. Sharp, M. Camplani, and J. Viner, Remote, Depth-Based Lung Function Assessment, IEEE Trans. Biomed. Eng., vol. 64, no. 8, pp. 1943-1958, Aug. 2017.

[10] X. Gao, X. Jiang, S. Bi, D. Matthews, S. Schaefer, and X. Liu, Measurement of the Complex Human Atrial-Ventricular Motions using Contact-Based Doppler Radar, 2019 IEEE 20th Wireless and Microwave Technology Conference (WAMICON), USA, 2019.

[11] T. Wartzek, C. Bruuser, M. Walter, and Steffen Leonhardt, Robust Sensor Fusion of Unobtrusively Measured Heart Rate, IEEE J. Biomed. Health Inform., vol. 18, no. 2, pp. 654-660, Mar. 2014.

[12] J. R. Raol, Multi-sensor Data Fusion with MATLAB. Boca Raton, FL: CRC Press, 2009.